Influences of Organometallic Polymer-Derived Catalyst Dispersion on SWNT Growth

SARAH LASTELLA,[1] HOICHANG YANG,[2] DAVID RIDER,[3] IAN MANNERS,[3]* PULICKEL M. AJAYAN,[4] CHANG Y. RYU[1]

[1]Department of Chemistry and Chemical Biology, Rensselaer Polytechnic Institute, Troy, New York 12180

[2]Rensselaer Nanotechnology Center, Rensselaer Polytechnic Institute, Troy, New York 12180

[3]Department of Chemistry, University of Toronto, Toronto, Ontario, Canada M5S3H6

[4]Department of Materials Science and Engineering, Rensselaer Polytechnic Institute, Troy, New York 12180

ABSTRACT: Catalyst formation kinetics of a ferrocene-containing homopolymer, poly-ferrocenylethylmethylsilane (PFEMS), is investigated as it relates to the catalysis of single walled carbon nanotubes (SWNTs) through a chemical vapor deposition (CVD) process. The formation and efficiency of the PFEMS-based iron catalyst is compared with that of the corresponding polystyrene (PS)-*b*-PFEMS diblock copolymer. The PFEMS homopolymer contains 23 wt % iron, while PS-*b*-PFEMS, with a 25 vol % PFEMS content, is only 6% iron. Despite its lower iron content, spin-cast PS-*b*-PFEMS films on SiO_2/Si substrates produce more active iron sites than spin-cast PFEMS films during CVD growth of SWNTs. This is related to the self-assembly of the block copolymer, where PFEMS domains are well dispersed in the PS matrix, which degrades at a CVD temperature of 920 °C to leave catalytically active elemental iron behind. On the contrary, the pure PFEMS films contain a high percentage of iron and silicon, which tend to transform into ceramic-coated iron at this high temperature, thus rendering the iron inactive towards SWNT growth. © 2007 Wiley Periodicals, Inc. J Polym Sci Part B: Polym Phys 45: 758–765, 2007
Keywords: iron catalyst; polyferrocenylsilane; single walled carbon nanotubes

INTRODUCTION

The organized growth of single walled carbon nanotubes has been realized through chemical vapor deposition (CVD), where the catalyst is typically deposited onto the substrate surface prior to the CVD process. Since catalyst particle size mediates SWNT growth in CVD processes, catalyst deposition and dispersion techniques are a critical step in SWNT synthesis.[1–4] Such depositions of iron, molybdenum, nickel, or cobalt have been prepared, where the nanoparticle diameter is directly related to the CVD furnace heating rate, catalyst matrix, and metal film thickness.[5] Recently, there has been focus on the precise control of metal nanoparticles via metal salt insertion into micelle centers[6] or by incorporating the metal into the structure of a polymer chain.[7–9] In either case, the metal is dispersed evenly from a solution over the substrate surface in a thin film, and the metal is separated into domains to allow for a controlled uniform particle size.[7–9] Although, it is clear that the organic material degrades during the CVD process

in these new solution-based techniques, no studies have been carried out to explore the explicit formation mechanism and the corresponding film and material characteristics effecting the catalyst formation. It is important to understand this mechanism(s) to develop the most efficient catalyst material for SWNT growth.

Here, we report catalyst formation kinetics of ferrocene-containing polymers, as it relates to SWNT yield through a methane CVD process. Specifically, the catalytic activity between a homopolymer, polyferrocenylethylmethylsilane (PFEMS) [Fig. 1(a)], and a diblock copolymer, polystyrene-*block*-ferrocenylethylmethylsilane (PS-*b*-PFEMS) [Fig. 1(b)] is compared to address the effects of polymer-based iron catalyst dispersion on SWNT growth. It was previously reported[7] that a spin-cast PS-*b*-PFEMS film acts as a template for the production of spherical iron domains. When

annealed beyond 500 °C, the PS matrix thermally degrades, leaving behind magnetic α-iron particles,[10–14] which are catalytically active toward SWNT synthesis. SWNT density on the substrate surface was shown to be dependent on the iron content per area.[7] However, catalyst loading on the surface is not the sole factor that manipulates SWNT yield during our CVD process. The catalyst matrix or support layer[15] plays a significant role in the formation of active catalyst particles. By comparing the different catalyst activity between PFEMS and PS-*b*-PFEMS thin catalyst films, we have investigated SWNT growth by formation of iron catalyst particles as a kinetic function of polymer matrix degradation, polymer film thickness, film continuity, and iron loading. We found that the PFEMS film itself is not a suitable template for SWNT growth because the iron domains are encapsulated with the ceramic-like residue of the silicon compound at high temperatures. Although nanotubes are produced in the PFEMS system, a lower percentage of the iron domains on the topmost surface are catalytically active, thus leaving behind an excess of unused and conductive particles which may interfere with electronic properties of constructed devices.
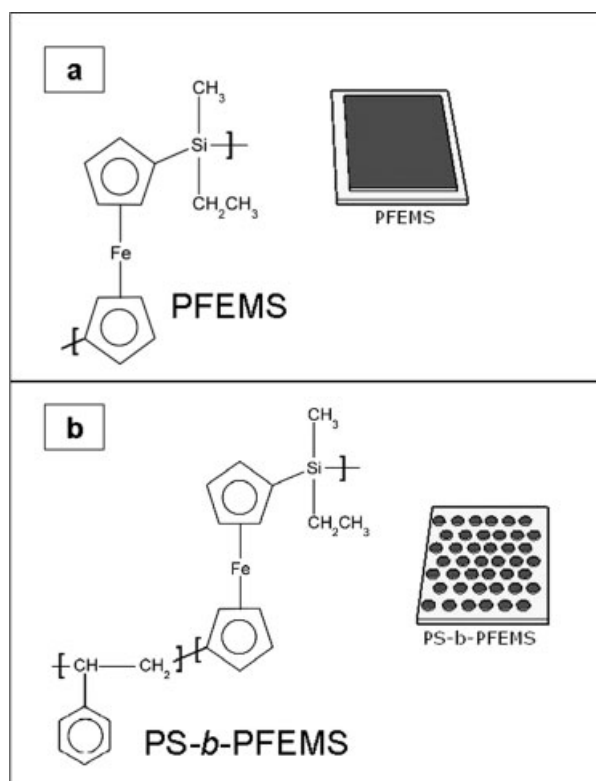
Figure 1. Chemical structures of PFEMS (a) and PS-*b*-PFEMS (b). The polymers are spin cast from toluene solutions to form a uniform film of PFEMS (a) and spherical domains of PFEMS in a PS matrix (b). These films are illustrated schematically beside the corresponding polymer where the PFEMS regions are represented in gray. Note that the PS matrix is not shown in the spin-cast film schematic of PS-*b*-PFEMS for clarity.

EXPERIMENTAL

Sample Preparation

PFEMS and PS-*b*-PFEMS were synthesized by methods previously described in Ref. 16. In this study, PFEMS had a number average molecular weight ($\overline{M}_n$) of 110,600 g mol^{-1} and a molecular weight distribution (MWD) of 2.02. PS-*b*-PFEMS was 25% PFEMS/vol and had a $\overline{M}_n = 38,600$ g mol^{-1} and MWD = 1.01

Dilute solutions (0.01 to 1 wt %) of PFEMS and PS-*b*-PFEMS were prepared in toluene and spin-cast on SiO$_2$/Si substrates or silicon nitride (Si$_3$N$_4$) membrane windows at 2500 rpm and at an accelerating rate of 2500 rpm/s. The 2.5 wt % solution of PS-*b*-PFEMS was spin-cast at 1000 rpm and 2500 rpm/s giving ~100 nm thick films. SWNTs were grown on the spin-cast films at 920 °C with methane in a CVD process previously described.[7]

Characterization

Samples were analyzed topographically with tapping-mode atomic force microscopy (TM-AFM)
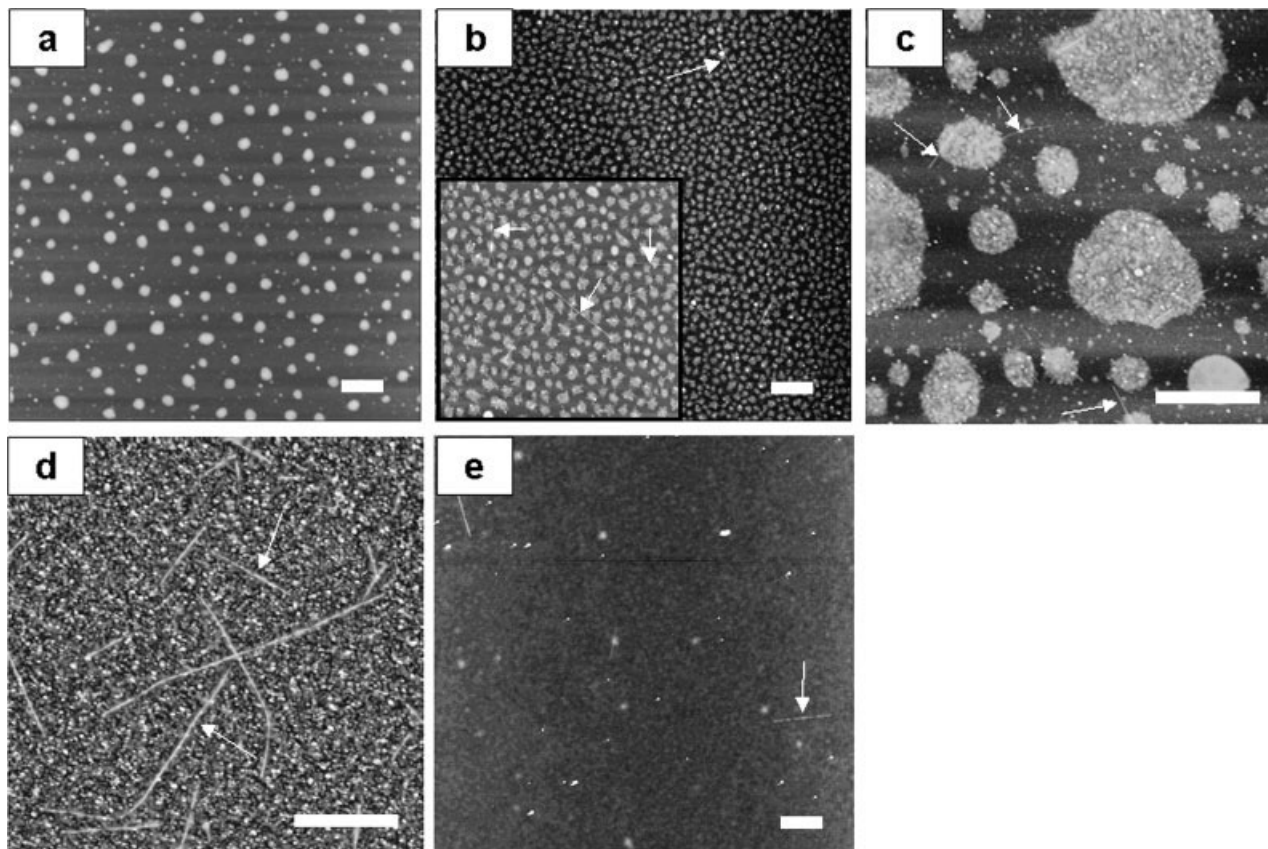
Figure 2. AFM topography images after CVD of PFEMS films cast from solution concentrations of (a) 0.01%, (b) 0.05%, (c) 0.1%, (d) 0.5%, and (e) 1.0%. The scale bars in white for each image represents 1 μm. A few SWNT bundles are marked by white arrows in each image. (a), (b), and (e) are 10×10 μm AFM scans, while (c) and (d) are 4×4 μm images to clearly illustrate the presence of nanotubes in each sample. The inset of (b) is a corresponding 4×4 μm image of the 0.05% sample. The average number of SWNT bundles/10×10 μm for each sample is 0.0, 2.8, 5.0, 32.0, and 2.6 for solution concentrations of (a) 0.01%, (b) 0.05%, (c) 0.1%, (d) 0.5%, and (e) 1.0%, respectively. These averages are also tabulated in Table 1.

(Multimedia Nanoscope IIIa, Digital Instrument/ Veeco Metrology Group) prior to and after CVD. Ten to fifteen randomly chosen regions on each sample surface were analyzed with 10×10 μm TM-AFM topographic images to determine the average SWNT density. The nanotube bundles were manually counted in each of the 10 (or more) AFM images for any single sample and averaged together. A standard deviation from the average was also calculated for each sample. The growth experiments were repeated another three times to ensure that the data was repeatable. The data represented here is one of these four sample sets. The residue on the samples after CVD was observed using transmission electron microscopy (Philips CM 12 TEM), operating at an accelerating voltage of 120 kV. The samples fabricated on Si_3N_4 membrane windows with center thickness of 50 nm were used for the TEM experiments. Specifically, to observe cross-sectional profiles of the CVD samples, the samples fabricated on Si_3N_4 membranes were embedded into an epoxy kit (Poly/bed 812, Polyscience) and cured at 60 °C for 1 day. Thin film blocks containing both a 50-nm Si_3N_4 window and cured epoxy were cut to $\sim$50 nm thick using an ultramicrotoming system (MT-XL, RMC).[17]

RESULTS AND DISCUSSION

Solution-processable polymer template effects on the iron catalyst formation and its activity in
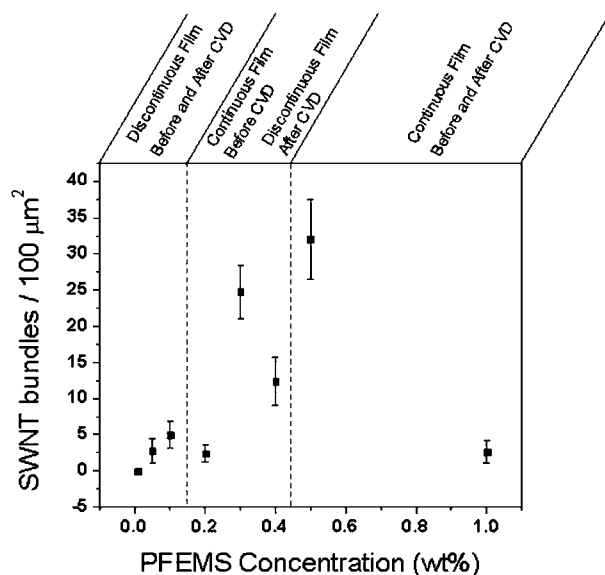
Figure 3. Average number of SWNTs in a 10×10 μm^2 area on the substrate surface with error bars for seven PFEMS homopolymer films with respect to the as-cast solution concentration. As-cast films are discontinuous below 0.1%.

spin-cast PFEMS films for the growth of SWNTs during the CVD process have been investigated by controlling the film thickness and continuity. PFEMS films were spin cast on SiO_2/Si substrates from various dilute solutions (0.01 to 1.0 wt %). The initial film thickness was determined from AFM cross-sectional height profiles. PFEMS samples of 0.01 and 0.05 wt % spin cast films did not fully cover the substrates, showing discrete island domains with lateral average sizes of $\sim$230 nm (0.043 μm^2) and $\sim$460 nm (0.168 μm^2), respectively. Above 0.05 wt % solu-

tions, the films formed continuous layers, ranging from 2.3 nm to 39 nm in thickness, with increasing polymer concentration in the spin cast solutions. However, after annealing at 920 °C during CVD, the spin-cast films with thicknesses below 14 nm became discontinuous. Figure 2 depicts TM-AFM topographs of five PFEMS films spin-cast from various solutions after undergoing CVD: three discontinuous (a–c) and two continuous (d,e) film samples after CVD. Also, the corresponding SWNT yield was plotted for seven different PFEMS films in Figure 3. Both Figures clearly indicate that as solution concentration increases, SWNT yield rises up to a concentration of $\sim$0.5 wt % and tends to drop above 0.5 wt %, as illustrated by the 1 wt % CVD sample with an initial film thickness of 39 nm.

Iron loading onto the surface was also characterized through polymer volume surface coverage and tabulated in Table 1. We found that the discontinuous film after spin coating shown in Figure 2(b) (0.05 wt %) supports a slightly larger number of iron atoms on the substrate than the 2.3 nm continuous film [Fig. 2(c)]: the discontinuous film is estimated to contain $\sim$8.89 $\times 10^{10}$ iron atoms per μm^2 while the continuous film supports only 6.82 $\times 10^{10}$ (Table 1). Since these iron quantities are fairly close in value compared with the other samples listed in Table 1, we can determine the physical properties of the film as it pertains to the formation of active catalysts for our CVD process while ignoring the effects of iron loading. The continuous film (5.0 $\pm$ 1.9 SWNTs per 100 μm^2) showed a nearly two-fold increase in SWNT growth yield over the discontinuous film (2.8 $\pm$ 1.6 SWNTs per 100 μm^2), indicating

Table 1. Average SWNT Bundle Growth Density Based on Iron Content and Polymer Film Properties[a]

Concentration	Film Continuity Before CVD	Film Continuity After CVD	No. of Fe Atoms (μm^2)	Film Thickness (nm)	No. of SWNTs (10×10 μm^2)
0.01% PFEMS	Discont.	Discont.	1.05×10^{10}	N/A	0.0 ± 0.0
0.05% PFEMS	Discont.	Discont.	8.89×10^{10}	N/A	2.8 ± 1.6
0.1% PFEMS	Cont.	Discont.	6.82×10^{10}	23	5.0 ± 1.9
0.5% PFEMS	Cont.	Cont.	5.04×10^{11}	17	32.0 ± 5.5
1% PFEMS	Cont.	Cont.	1.16×10^{12}	39	2.6 ± 1.5
0.01% PS-b-PFEMS	Discont.	Discont.	5.90×10^{9}	N/A	0.0 ± 0.0
0.5% PS-b-PFEMS	Cont.	Cont.	1.81×10^{11}	17	24.0 ± 4.9
2.5% PS-b-PFEMS	Cont.	Cont.	3.32×10^{11}	97	1.0 ± 0.0

[a] Discont. and Cont. refer to discontinuous and continuous polymer films, respectively.

that catalyst particle formation from a continuous film results in twice the number of active catalysts observed in the discontinuous films. When the continuous layer structure of an initial PFEMS film is maintained at this high CVD temperature, a larger percentage of iron can be exposed to the carbon source (methane) because of the higher aerial density of iron particles compared to that in a discontinuous layer. However, in the case of a thicker film such as the 39 nm thick sample [Fig. 2(e)], most iron beneath the film surface is likely blocked from the active surface area of the metallic clump and is unable to contribute to the catalysis of SWNTs. Thus, SWNT density is not only a function of iron loading but also of the efficiency to form active iron sites during the CVD process, which is largely influenced by the original film thickness.

In ferrocene-containing polymer-based templates for SWNT growth, iron particle formation is also affected by iron dispersion in the hydrocarbon matrix. The PFEMS homopolymer contains 23 wt % iron, while PS-*b*-PFEMS with a 25% volume ratio of PS to PFEMS is only 6% iron. Thus, the block copolymer is composed of statistically less iron than its corresponding homopolymer and should ultimately fall short of PFEMS with respect to SWNT production, if iron dispersion effects are ignored. In fact, we have found that although there are fewer iron atoms in a PS-*b*-PFEMS thin film, a higher percentage of the atoms are catalytically active in the block copolymer. Homo- and block copolymer thin films of 17 nm in initial (spin-cast) thickness after CVD are shown in Figures 2(d) and 4 after undergoing CVD, respectively. Interestingly, the SWNT density on both surfaces is approximately equal, even though iron loading on the homopolymer surface (5.04×10^{11} atoms/ μm^2) is approximately three-fold that of the block copolymer (1.81×10^{11} atoms/μm^2). The PFEMS homopolymer film yields an average of 32.0 ± 5.5 bundles/100 μm^2, and thus we can predict that ~11 bundles will grow from the corresponding PS-*b*-PFEMS sample. However, an average of (24.0 ± 4.9) bundles/100 μm^2 was observed on the block copolymer catalyzed samples, more than twice the predicted growth density. Therefore, it can be estimated that nanoscale-dispersion of the PFEMS-based iron in a polystyrene matrix via block copolymer self-assembly produces over two times more active catalysts than a homogeneous film of nondiscrete iron particles from a spin-cast PFEMS film.
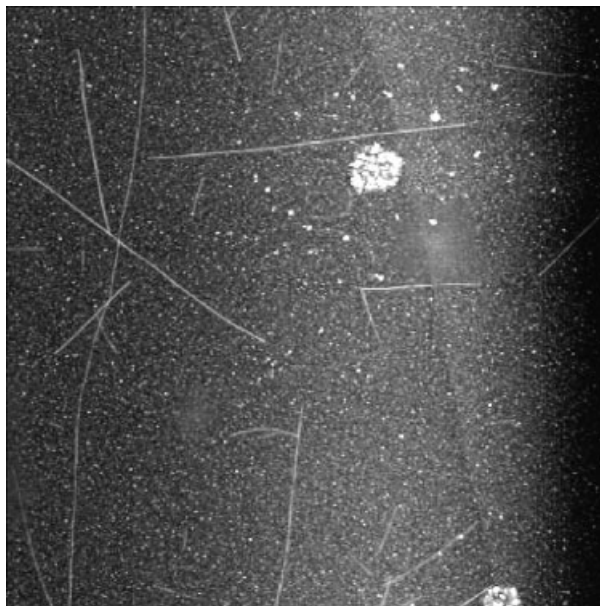
Figure 4. AFM image ($10 \times 10 \ \mu m^2$) of SWNT growth from a 0.5 wt % cast PS-*b*-PFEMS thin film (thickness = 17 nm). The average number of SWNTs was calculated to be 24.0 ± 4.9, which is also documented in Table 1.

There are two major factors contributing to this observed catalytic activity: iron particle generation (distribution) and catalyst encapsulation. It was previously shown that upon heating to temperatures beyond 900 °C, iron atoms in a polyferrocenylsilane-based matrix were released from the polymer backbone and agglomerated with a bimodal size distribution.[18] The large aggregates were explained to grow at grain boundaries caused by ceramic formation at these temperatures. Such generation may be inhibited in microphase-separated block copolymer films due to well-dispersed iron-rich nano-domains which only give rise to iron nanoparticles that are of insufficient diameter to produce ceramics with grain boundaries. The TEM results for spin-cast PFEMS and PS-*b*-PFEMS films from 0.5 wt % solutions before and after CVD processing are illustrated in Figure 5. First, in-plane TEM analysis for the spin-cast samples revealed inside film structure, which had not been detected by AFM. The large variation in iron domain size within the as-cast homopolymer film is evident in Figure 5(a) when compared with the block copolymer film in Figure 5(b), where the iron-rich domains are indicated by the dark regions in the TEM images (white arrows in Fig. 5). After CVD, the homopolymer left traces of the silane polymer
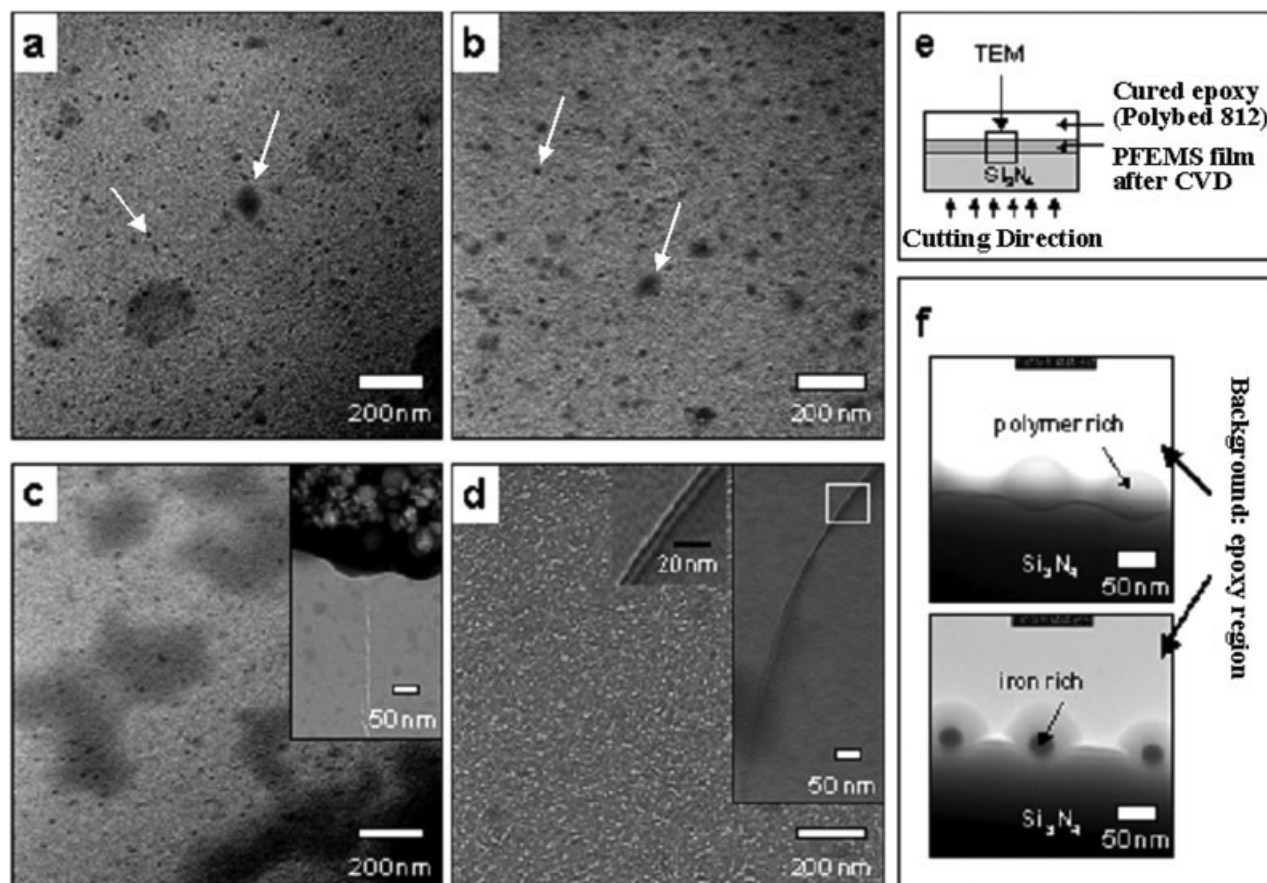
Figure 5. TEM micrographs of PFEMS and PS-*b*-PFEMS films spin-cast onto a Si$_3$N$_4$ window from 0.5 wt % toluene solutions. The as-cast films are represented in (a) and (b) for PFEMS and PS-*b*-PFEMS, respectively. The films after CVD are shown in (c) and (d) for PFEMS and PS-*b*-PFEMS, respectively. The PFEMS as-cast film (a) shows large and small agglomerates of iron seen as dark spots in the image marked by white arrows. The block copolymer (b), on the other hand, shows a more uniform size distribution of these iron-containing domains (white arrows). After CVD, PFEMS leaves behind ceramic particles which are seen more clearly in the inset of (c). PS-*b*-PFEMS leaves no visible residue or ceramic formation on the TEM window [(d) and inset]. (e) Schematic of ultramicrotoming experiment for cross-sectional TEM analysis where an epoxy is cured on top of the PFEMS film after CVD. (f) Cross-sectional TEM micrographs of the PFEMS film after CVD: top image shows the spheres of ceramic left from the PFEMS film, and the bottom image shows the iron particles trapped inside the ceramic material.

backbone, which constitutes 77% by weight of the entire polymer chain. This remaining material showed undulated and segregated islands on the Si$_3$N$_4$ substrate [Fig. 5(c)], indicating ceramic-like residues.[19–21] In this case, though small iron nanoparticles from the as-cast film still remained after CVD, few SWNTs were detected around the large aggregated clumps [Fig. 5(c) inset]. On the contrary, there was no indication of a film containing any large iron particles in the block copolymer sample after CVD [Fig. 5(d)]. SWNTS

on the PS-*b*-PFEMS coated Si$_3$N$_4$ window were found without large iron or ceramic particles [Fig. 5(d) inset], unlike the homopolymer grown SWNTs. Thus, the block copolymer-based template provides a matrix suitable for the production of only small iron particles, while the homopolymer allows for both large and small particle formation. Secondly, the polyferrocenylsilanes have been reported to form ceramic particles at temperatures above 500 °C.[18–21] TEM results illustrate that the iron [dark regions in Fig. 5(c)

inset] are nucleated and generated near the grain-boundaries of the ceramic-like residues. Interestingly, the ceramic-like residues were only displayed in the PFEMS homopolymer films, where some regions contained encapsulated iron particles [Fig. 5(e)], while no ceramic material was present in the spin-cast block copolymer film [the inset in Fig. 5(d)]. It is concluded that the PS matrix acts not only as a dispersing agent for PFEMS, but also prevents dispersed PFEMS domains from agglomerating into encapsulated iron particles. Although PFEMS provides a greater amount of iron compared to the copolymer, only a fraction of the particles in the homopolymer film are both small enough and exposed to the CVD environment to catalyze the growth of SWNTs. The block copolymer is, therefore, able to more efficiently produce SWNTs.

We showed in an earlier study[7] that SWNT yield drops at film thicknesses around 100 nm due to an agglomeration of iron into large and therefore in-active SWNT catalysts. We can compare these results with those observed for a 39 nm PFEMS film [Fig. 2(e)], where the growth for both samples is significantly low ($\sim$1 tube per 100 μm^2). PFEMS reaches its growth limit at a film thickness less than half that observed for the block copolymer. However, iron loading for a 97 nm thick block copolymer film is 3.32 $\times$ 10^{11} atoms/μm^2, approximately a third of the amount present in the 39 nm thick PFEMS homopolymer film (1.16 $\times$ 10^{10} atoms/μm^2). Clearly two different limiting factors are inhibiting the formation of discrete, exposed catalyst domains in these two noncatalytic polymer films. The iron rich PFEMS homopolymer film fully degrades and collapses to create large iron domains during CVD, which begin to exceed feasible SWNT production conditions at spin-cast film thicknesses of 39 nm. PS-*b*-PFEMS, however, contains a limited amount of iron even in thick ($\sim$100 nm) films. Therefore, it is not the formation of large iron particles, but the lack of complete degradation near the bottom of the thick polymer film due to short exposure ($\sim$20 min) to the high CVD temperatures that ultimately hinders SWNT growth from the thick block copolymer films.

CONCLUSIONS

SWNT growth is dependent on catalyst formation, which is a function of film thickness and film continuity in PFEMS films. The formation of iron particles from both polymer-based catalysts is a kinetic process directly dependent on our CVD process conditions. As a result of the rapid kinetic formation, the discrete nanoscale dispersion of PFEMS iron domains via block copolymer self-assembly allows for better particle control than the continuously dispersed iron in PFEMS homopolymer films. Based on SWNT yield at equal atomic catalytic loadings, we also found that iron present in the block copolymer shows higher catalytic activity than that present in the homopolymer film, which may be attributed to the nanoscale-dispersion of the catalytic iron domains in the polystyrene matrix. These results are substantiated by the observation that iron becomes encapsulated in the pure PFEMS films during CVD and that only the block copolymer produces a single, fairly uniform catalyst particle size distribution.

REFERENCES AND NOTES

1. Wang, Y. Y.; Gupta, S.; Nemanich, R. J Appl Phys Lett 2004, 85, 2601.
2. Jung, Y. J.; Homma, Y.; Ogino, T.; Kobayashi, Y.; Takagi, D.; Wei, B.; Vajtai, R.; Ajayan, P. M. J Phys Chem B 2003, 107, 6859.
3. Li, Y.; Kim, W.; Zhang, Y.; Rolandi, M.; Wang, D.; Dai, H. J Phys Chem B 2001, 105, 11424.
4. Cheung, C. L.; Kurtz, A.; Park, H.; Lieber, C. M. J Phys Chem B 2002, 106, 2429.
5. Seidel, R.; Duesberg, G. S.; Unger, E.; Graham, A. P.; Liebau, M.; Kreupl, F. J Phys Chem B 2004, 108, 1888.
6. Fu, Q.; Huang, S.; Liu, J. J Phys Chem B 2004, 108, 6124.
7. Lastella, S.; Jung, Y. J.; Yang, H.; Vajtai, R.; Ajayan, P.M.; Ryu, C. Y.; Rider, D.; Manners, I. J Mater Chem 2004, 12, 1791.
8. Hinderling, C.; Keles, Y.; Stockli, T.; Knapp, H.; de los Acros, T.; Oelhafen, P.; Korczagin, I.; Hempenius, M. A.; Vansco, G. J.; Pugin, R.; Heinzelmann, H. Adv Mater 2004, 16, 876.
9. Lu, J. Q.; Kopley, T. E.; Moll, N.; Roitman, D.; Chamberlin, D.; Fu, Q.; Liu, J.; Russell, T. P.;

Rider, D. A.; Manners, I.; Winnik, M. Chem Mater 2005, 17, 2227.

10. Ni, Y.; Rulkens, R.; Manners, I. J Am Chem Soc 1996, 118, 4102.

11. Temple, K.; Massey, J. A.; Chen, Z.; Vaidya, N.; Berenbaum, A. M.; Foster, D.; Manners, I. J Inorg Organomet Polym 1999, 9, 189.

12. Manners, I. Chem Commun 1999, 10, 857.

13. Manners, I. Science 2001, 294, 1664.

14. Temple, K.; Kulbaba, K.; Power Billard, K. N.; Manners, I.; Leach, K. A.; Xu, T.; Russell, T. P.; Hawker, C. J Adv Mater 2003, 15, 297.

15. Zhang, R. Y.; Amiani, I.; Baker, J.; Tresek, J.; Tsui, R. K. Nano Lett 2003, 3, 731.

16. Rider, D. A.; Cavicchi, K. A.; Power-Billard, K. N.; Russell, T. P.; Manners, I. Macromolecules 2005, 38, 6931.

17. Yang, H.; Sa, U.; Kang, M.; Ryu, H. S.; Ryu, C. Y.; Cho, K. Polymer 2006, 47CID, 3889.

18. Ginzburg, M.; MacLachlan, M. J.; Yang, S. M.; Coombs, N.; Coyle, T. W.; Raju, N. P.; Greedan, J. E.; Herber, R. H. J Am Chem Soc 2002, 124, 2625.

19. Petersen, R.; Foucher, D. A.; Tang, B. Z.; Lough, A.; Raju, N. P.; Greedan, J. E.; Manners, I. Chem Mater 1995, 7, 2045.

20. Sun, Q. H.; Lam, J. W. Y.; Xu, K. T.; Xu, H. Y.; Cha, J. A. K.; Wong, P. C. L.; Wen, G. H.; Zhang, X. X.; Jing, X. B.; Wang, F. S.; Tang, B. Z. Chem Mater 2000, 12, 2617.

21. Tang, B. Z.; Petersen, R.; Foucher, D. A.; Lough, A.; Coombs, N.; Sodhi, R.; Manners, I. J Chem Soc Chem Commun 1993, 6, 523.